Positron-Annihilation Study of the Electronic-Structure of Uru2si2

Rozing, G.J.; Mijnarends, P.E.; Menovsky, A.A.; Dechatel, P.F.

DOI
10.1103/PhysRevB.43.9523
Publication date
1991

Published in
Physical Review. B, Condensed Matter

Positron-annihilation study of the electronic structure of URu_2Si_2

G. J. Rozing and P. E. Mijnarends
Netherlands Energy Research Foundation ECN, 1755 ZG Petten, The Netherlands

A. A. Menovsky and P. F. de Châtel
Natuurkundig Laboratorium, University of Amsterdam, 1018 XE Amsterdam, The Netherlands
(Received 23 October 1990)

Measurements of the two-dimensional angular correlation of annihilation radiation (2D-ACAR) were performed on oriented single crystals of URu_2Si_2. The spectra, obtained with integration along four different symmetry directions, display anisotropic structure in fair agreement with a previous calculation of the two-photon momentum distribution. In particular, the contribution of the f-ligand hybridized electron states is clearly observed and reasonably well described by the band calculation. The 2D-ACAR distribution remains unchanged as the temperature is increased from 6 K in the Fermi-liquid state to 72 K, which is just above the coherence temperature. The inhomogeneity of the positron density in the unit cell complicates the Lock-Crisp-West (LCW) analysis of the experiments in terms of Fermi-surface features. Nevertheless, the disagreement between theory and experiment after LCW folding indicates that the Fermi surface as predicted by local-density-approximation band theory does not apply.

I. INTRODUCTION

This paper focuses on the electronic structure of the heavy-fermion system URu_2Si_2—in particular, its electron momentum distribution. Although the effective electron mass, deduced from specific-heat experiments, is not so large in URu_2Si_2 ($\gamma=65$ mJ/K^2 mol formula unit),[1,2] this compound has received considerable attention, as it is the first heavy-fermion system in which the coexistence of magnetic order and superconductivity was observed.[3–5] The relevance of band theory has often been questioned with respect to heavy-fermion systems since the many-body correlations are not expected to be adequately described by the local-density approximation (LDA). And, indeed, band masses obtained from band-structure calculations are usually smaller than the measured effective masses by one or two orders of magnitude. However, despite the mass discrepancy, the calculated Fermi surface was found to yield a satisfactory explanation of the experimental data provided by de Haas–van Alphen (dHvA) measurements for $CeSn_3$ (Ref. 6) and UPt_3.[7]

It has been shown for a wide range of materials that positron annihilation, like the dHvA effect, can be used to assess the validity of the calculated Fermi surface by measuring the two-dimensional angular correlation of the annihilation radiation (2D-ACAR). An extensive review has been given by Berko.[8] In addition, a 2D-ACAR measurement provides information about the shape of the electronic wave functions. In order to extract such information from 2D-ACAR measurements on single-crystalline URu_2Si_2, we have previously calculated[9] the two-photon momentum distribution for positron annihilation for this compound, using the eigenvalues and wave functions provided by a LDA band calculation. We showed that the crystal structure of URu_2Si_2 favors an overlap of the positron wave function with the U f electrons. Thus, in spite of the tightly bound nature of the f-electron states, it appears feasible to study the Fermi-liquid state in URu_2Si_2 by the positron-annihilation technique.

In this paper the results are presented of 2D-ACAR experiments on oriented single crystals of URu_2Si_2. An analysis of the experiments yields two different conclusions with respect to the LDA band calculation: The shape of the hybridized f-ligand wave functions is rather well described by theory, whereas the calculated Fermi surface is not in agreement with the measurements. The 2D-ACAR technique, unlike the various methods based on quantum oscillations, has the additional advantage that high temperatures, with an accompanying decrease of the lifetime of the electron states, do not hamper the measurements. It will be shown that, despite the occurrence of magnetic ordering at 17 K, the transition from coherent to incoherent electron scattering around 60 K, and crystal-field effects, the measured distributions do not reflect a clear temperature dependence of the electronic structure.

II. EXPERIMENTAL DETAILS

Menovsky *et al.*[10] have given a detailed description of the method employed to grow the two single crystals of URu_2Si_2 used in this work. From these crystals, called A and B, respectively, four samples were cut by spark erosion. The samples were designated $A0$, $A1$, $A2$, and $B3$. In view of the mean implantation depth of the positrons in this material of approximately 25 μm, attempts were made to remove the surface layer by chemical etching and mechanical polishing. The surfaces were studied with a scanning electron microscope (SEM). Although the etching, using nitric acid with some hydrofluoric acid

added, was found to be very difficult, the surface layer of samples $A1$ and $A2$ could be successfully removed. From SEM microprobe x-ray analysis before and after etching, it was inferred that the removed layer was slightly oxidized. Only a single lifetime component could be resolved in positron-lifetime spectra measured in these samples. The lifetime was 190 ps for the samples as spark cut and showed a significant decrease of 10 ps after etching. This indicates that the surface layer contained deformation damage as a result of the spark erosion. Unfortunately, the results of the etching process were less satisfactory for samples $A0$ and $B3$. Therefore, these samples were polished mechanically using 1-μm diamond powder, resulting in a decrease of the positron lifetime with respect to the untreated sample by only 3 ps, which is hardly significant. The defect concentration in the surface layer thus appears to be higher for these two samples than for the etched samples. The mechanically polished surfaces offered the possibility to study the chemical composition. The composition was found to be constant over the surface within 1 at. %, except for small U-rich segregates (most likely U oxides) which cover less than 1% of the surface of the samples. Unlike the samples cut from crystal A, a mosaic spread of 0.5° was observed in $B3$. This mosaic spread is small enough not to perturb the 2D-ACAR measurements. It was found that all samples were extremely brittle after both etching and polishing.

The angle between the two 511-keV photons emitted upon annihilation of a positron in a solid deviates slightly from 180°. The deviation, of the order of 1°, is a direct measure of the transverse components (p_y,p_z) of the electron-positron pair momentum $\mathbf{p}=(p_x,p_y,p_z)$ before annihilation, if p_x lies along the direction of photon emission.[8] The two-dimensional angular correlation is measured by observing coincidences between two position-sensitive detectors of the Jeavons type placed on either side of the sample.[11] The measured coordinates of the annihilation quanta directly provide p_y and p_z. The accumulation of 10^7-10^8 coincidences yields the two-dimensional angular correlation $N(p_y,p_z)$ after correction for the background and the momentum sampling function. The latter takes into account the momentum-dependent efficiency by which the angular correlation is measured.[8] The third momentum component p_x yields a Doppler shift of the photon energies of the order of 1 keV. Since the detectors used cannot discriminate energies on this scale, a 2D-ACAR experiment determines a projection of the two-photon momentum distribution $\rho_{2\gamma}(\mathbf{p})$:

$$N(p_y,p_z)=\text{const}\times\int\rho_{2\gamma}(\mathbf{p})dp_x\ , \tag{1}$$

where the integration direction is determined by the orientation of the sample. The sample is subject to a magnetic field of ~ 6 T along the p_z direction, which guides the positrons to the sample.[11] This field is weak enough not to induce important changes in the macroscopical properties of URu_2Si_2.[12,13] The crystal structure[3] of URu_2Si_2 is body-centered tetragonal with $c=9.582$ Å and $a=4.124$ Å at 4.2 K.

As the 2D-ACAR experiments presented in this paper cover a long period of time (three years), the details of the measurements reflect both the progress in sample preparation and further improvement of the apparatus. The characteristics of the measurements, presented in this paper, are summarized in Table I. The first measurements were obtained from sample $A0$ as spark cut. Measurements with integration directions [100] and [110] were performed at 8 K, in the magnetically ordered state, and at 20 K, just above the ordering temperature. Figure 1 shows the integration directions with respect to the Brillouin zone. The mechanically polished sample $B3$ was used to measure the momentum distribution integrated along the [001] axis. The installation of a new positron source with a smaller radioactive area allowed measurements on the small etched sample $A1$. At the same time a newly developed sample holder was employed to increase the temperature range. On sample $A1$, 2D-ACAR measurements were performed at 6 K with integration directions [001] and [101] and at 72 K with integration along the [001] direction (please remember that the crystallographic direction [101] lies along the vector $(2\pi/a,0,2\pi/c)$). In the latter high-temperature measurement only 10^7 coincidences were

TABLE I. Summary of the characteristics of the 2D-ACAR measurements including the surface treatment of the samples.

Integration direction	T (K)	Sample	Treatment	Number of counts ($\times 10^6$)
[100]	8	$A0$	a	60
[100]	20	$A0$	a	31
[110]	8	$A0$	a	60
[110]	20	$A0$	a	55
[001]	8	$B3$	b	40
[001]	6	$A1$	c	33
[001]	72	$A1$	c	10
[101]	6	$A1$	c	47

[a]None.
[b]Mechanically polished.
[c]Chemically etched.

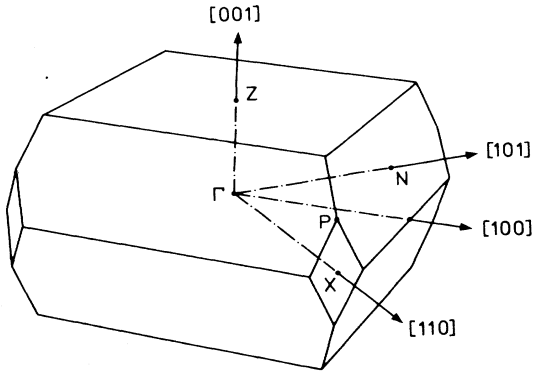

FIG. 1. Brillouin zone of URu_2Si_2 with the four integration directions selected in the 2D-ACAR experiments.

collected and, consequently, it does not provide the same level of accuracy as the other measurements (cf. Table I). Sample $A2$ was used only in the positron-lifetime measurements. The momentum resolution differs for the various experiments due to the different sample-detector distances, the installation of the smaller positron source, and the different sample temperatures yielding different contributions of the positron thermal motion to the momentum resolution. These differences are greatly suppressed by the application of the same smoothing procedure to all results. The experimental data displayed in the figures are subject to an effective angular resolution (including smoothing) of approximately 0.6 mrad in both directions, equivalent to an effective momentum resolution of 0.082 a.u., unless quoted otherwise. The channel width is determined by the sample-detector distances and ranges from 0.231 to 0.211 mrad, except for the [101] integration, which was measured on a finer mesh with a channel width of 0.116 mrad. Following common practice in ACAR studies, in this paper we will use milliradians as the unit of momentum (1 a.u. = 7.297 mrad).

III. RESULTS

The measured 2D-ACAR distributions are rather smooth, with their maximum in the center corresponding to zero projected momentum. At first sight they do not

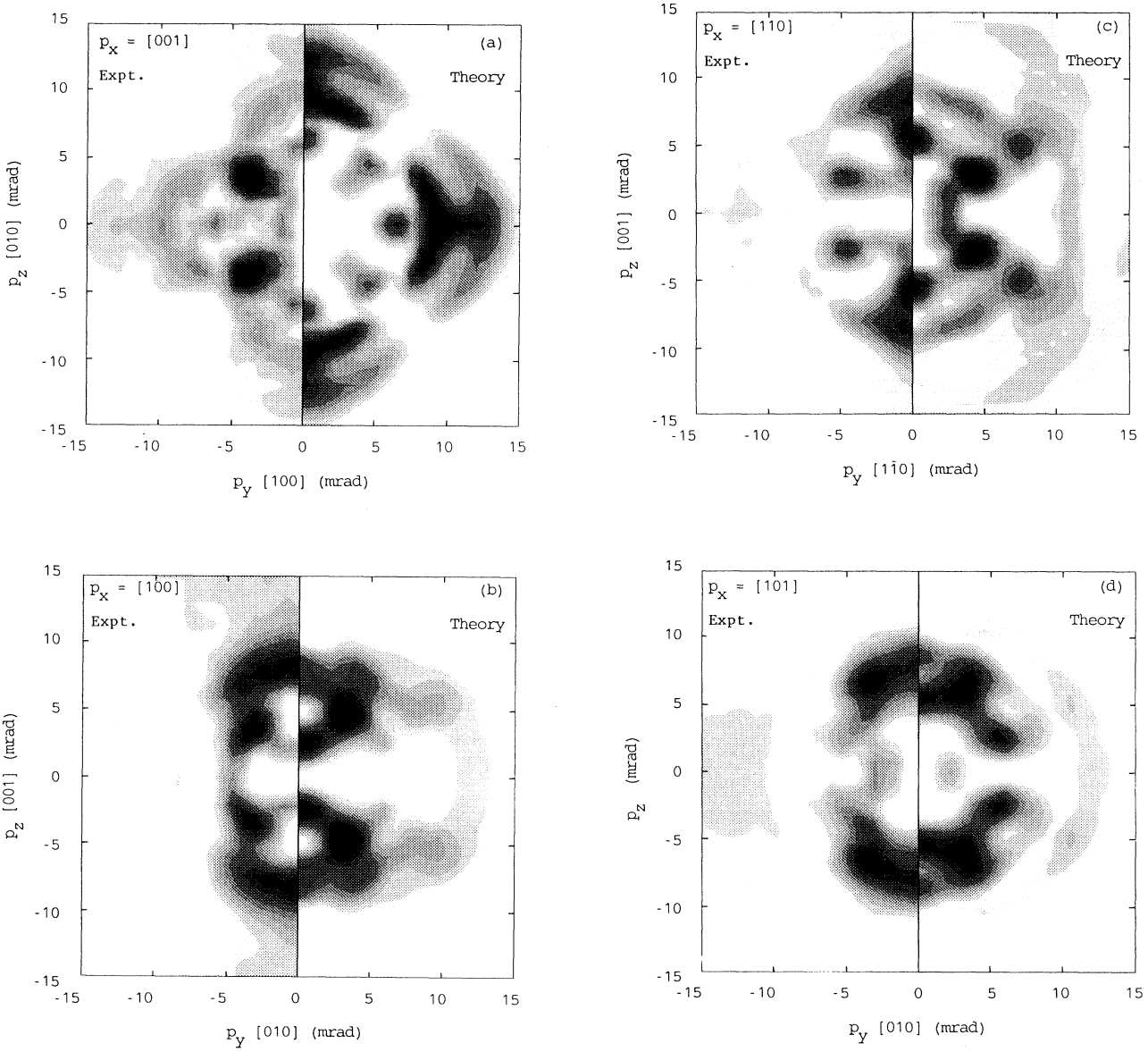

FIG. 2. Anisotropy in the measured (left) and calculated (right) 2D-ACAR distributions with integration along the (a)–(d) [001], [100], [110], and [101] directions, respectively. The distributions shown were obtained with the samples $A0$ and $A1$ (see Table I) kept at low temperatures (6 or 8 K). The shading changes linearly with the amplitude of the anisotropy. Black corresponds to the maximum value and white to values close to 0. The scaling for theory and experiment was performed independently. Please remember that the direction [101] lies along the vector $(2\pi/a, 0, 2\pi/c)$. Hence, the p_z axis in (d) does not coincide with a crystallographic symmetry direction.

display any structure indicative of electronic-structure effects. In order to bring out anisotropic features, the customary procedure is applied of subtracting an isotropic function. This isotropic function $R(p)$ is defined as the minimum value in $N(p_y,p_z)$ found on the circle $p_y^2+p_z^2=p^2$. The residual anisotropic distribution is therefore always positive. All four integration directions provide 2D-ACAR distributions with a rich anisotropic structure, which is displayed in the left halves of Figs. 2(a)–2(d). The total content of the anisotropy,

$$\int\int\{N(p_y,p_z)-R[(p_y^2+p_z^2)^{1/2}]\}dp_y dp_z ,$$

amounts to 4–6 % of the content of the 2D-ACAR distribution, except for the [110] integration direction, which yields 11% total anisotropy. The maximum values in the anisotropic parts range from 1.5% for the [110] integration to 2.5% for the [101] integration direction, measured relative to $N(0,0)$. The contribution from annihilations with core electrons complicates a direct comparison of theory with experiment, as the core is not included in the calculation of the two-photon momentum distribution. However, filled core shells can be assumed to yield an isotropic momentum distribution, so that the anisotropic structure in the 2D-ACAR measurements is predominantly due to the band electrons. The calculated anisotropies, determined from the appropriate integrals of the three-dimensional momentum distribution by the subtraction procedure described above, are displayed in the right halves of Figs. 2(a)–2(d) for comparison with the measurements. The anisotropic structure, with a content of 8% for the calculated [110] integration and 6% for the remaining theoretical integrations, is indeed observed in the experimental distributions. The anisotropic structure at large momenta ($p>6$ mrad) in the [001] and [110] integrations is especially noteworthy. Although the calculated amplitude is too large by at least a factor of 2 compared with the structure present at small momenta, the shape of the structure is in striking agreement with experiment. Also, closer to the origin, much of the anisotropy predicted by theory is observed in the experimental distributions. To a large extent, the structural features in the theoretical and experimental anisotropies have the same location and shape and differ only in amplitude. Exceptions are found in the experimental data of the [100], [110], and [101] integration directions near $p_y=0$ mrad and $p_z=\pm 8$ mrad. The observed maxima are missing, or at least smaller, in the calculations. Also, the locations of the maxima in the [100] distribution at $p_y=p_z=\pm 3$ mrad are calculated to lie at values of p_z which are too high.

In order to evaluate the influence of the positron on the two-photon momentum distribution, we have substituted a constant for the positron wave function in the calculation. The result equals the momentum distribution of the electrons. We observe a slightly larger momentum density at large momenta, but roughly the same anisotropic structure after integration as was obtained from the two-photon momentum distribution calculated with the full positron wave function. It can thus be concluded that the anisotropic effects observed in Fig. 2 are characteristic of the purely electronic momentum distribution.

In order to estimate the sensitivity of the calculated 2D-ACAR distributions to the geometry of the Fermi surface, shifts have been applied to the Fermi energy. The differences in the anisotropy between the theoretical and experimental distributions are to some extent reduced when the Fermi energy is lowered by 10–20 mRy. This modifies the Fermi surface drastically. In the calculated [001] distribution at $|\mathbf{p}|=6$ mrad the maxima along the $\langle 100\rangle$ axes become smaller, but the calculated anisotropy at large momenta remains too large. Despite the changes in the Fermi energy, the calculated momentum density at $p_z=\pm 8$ mrad for the other integration directions is still too small compared with the measurements. The conclusion is justified that the anisotropic structure found experimentally, which, as shown above, is of electronic nature, mainly originates from the nonsphericity of the occupied electron wave functions rather than from the Fermi surface.

In the measurements at elevated temperatures (20 and 72 K, respectively) no differences with the corresponding low-temperature distributions could be detected. In spite of its poor statistics, the measurements at 72 K, with the integration along the [001] direction, show the same large-momentum anisotropy as is present in the left half of Fig. 2(a).

The two low-temperature measurements on different samples with integration along the [001] direction reveal marked differences. Whereas at small momenta the two samples yield the same anisotropic structure with approximately equal amplitudes, the distribution in sample $B3$ lacks the anisotropic structure that is present at large momenta in the measurement on sample $A1$. The measured value of the positron lifetime in sample $B3$, which is significantly higher than in the chemically polished sample $A1$ (187 versus 180 ps), suggests the presence of defects capable of trapping positrons in the surface layer of the sample, which does not seem unrealistic in view of the mechanical polishing. Therefore, we attribute the absence of anisotropy at large momenta in sample $B3$ to the presence of defects. Consequently, in Fig. 2(a) the results are shown of the measurement on sample $A1$.

The hybridized U f bands near the Fermi energy are of special interest to us, since they are responsible for the heavy-fermion character of URu_2Si_2. Their contributions to the two-photon momentum distribution can be identified in our calculations and are found to be especially large for $p>6$ mrad along the $\langle 100\rangle$ axes. The anisotropic structure observed at $p>6$ mrad after integration along the [001] direction is mainly due to these electron states. The good agreement with experiment with respect to this feature is therefore especially satisfying. A curve showing the difference between cuts through the 2D-ACAR distribution along the $\langle 100\rangle$ and $\langle 110\rangle$ axes is shown in Fig. 3 for both theory and experiment. This figure conveniently displays the contribution of the f-electron states in the momentum region from 6 to 15 mrad. The agreement between theory and experiment, in particular with respect to the negative peak at ~ 5 mrad, is improved by a decrease of the Fermi energy by 20 mRy as shown in Fig. 3(a). The experiment seems to confirm the small negative tail at ~ 18 mrad. The experimental

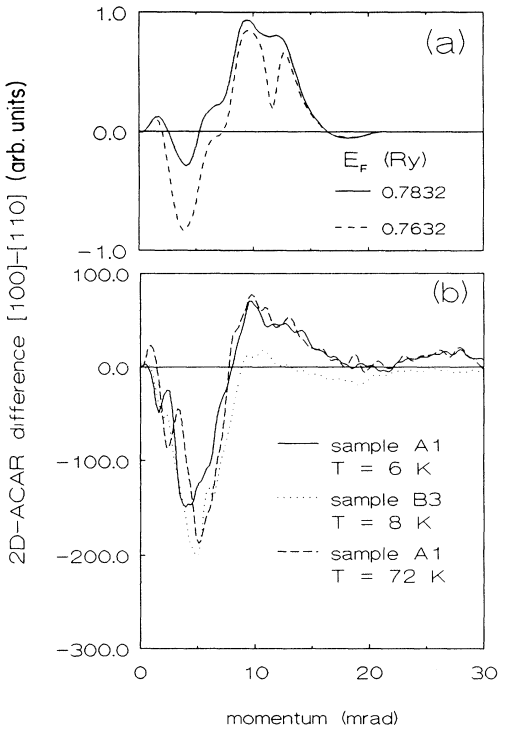

FIG. 3. Difference curves of the cuts along the ⟨100⟩ and ⟨110⟩ directions through the 2D-ACAR distributions, measured with integration along the [001] axis. (a) Theoretical curves are plotted for the self-consistent Fermi energy and the Fermi energy lowered by 20 mRy. (b) Experimental data are displayed for measurements on sample *A*1 at 6 and 72 K and on sample *B*3 at 8 K. The experimental 2D-ACAR distributions have been normalized to equal total contents. Both theory and experiment were convoluted with a Gaussian with 0.7 mrad full width at half maximum (FWHM).

curves show again, on the one hand, the absence of structure at large momenta for sample *B*3 (the measurement at 8 K) and, on the other hand, the similarity of the measurements at 6 and 72 K.

Although the anisotropy in the 2D-ACAR distribution in itself does not have a physical meaning, it shows that the overall agreement between theory and experiment is reasonable, while the structure related to the *f* states is represented satisfactorily by the band calculation. As shifts of the Fermi energy show that the anisotropy is rather insensitive to the shape of the Fermi surface, further analysis of the 2D-ACAR experiments is accomplished by invoking the Lock-Crisp-West (LCW) theorem.[14] In an LCW analysis ordinates of the 2D-ACAR distribution in points that differ by the projection of a reciprocal-lattice vector are summed to yield the two-dimensional LCW distribution.[8] In the hypothetical case of a flat positron wave function, which is not too bad an approximation in close-packed materials, this LCW distribution would equal the integrated number of occupied bands, thus reflecting a projection of the Fermi surface. In URu_2Si_2, however, the positron charge is quite inhomogeneously distributed over the unit cell, with a large positron density near the U sites, which hampers a straightforward interpretation of the LCW distributions. In our calculations of the theoretical 2D LCW distributions[9] we found slow variations originating in the inhomogeneity of the positron distribution in the unit cell, which dominate over the structure related to the Fermi surface. We applied the LCW procedure to the measured 2D-ACAR distribution and found that the effects caused by the positron wave function are also present in the experimental LCW distributions.[15] No additional structure could be distinguished for the [001], [100], and [110] integrations. In the calculated LCW distributions the Fermi-surface-related structure is indeed very small for the [001] and [100] integrations, since the two electron surfaces at Γ and the two hole surfaces at *Z* overlap in projection. The [110] integration direction does separate the projections of Γ and *Z*, but is severely affected by the positron wave-function effect. Figure 4 displays the

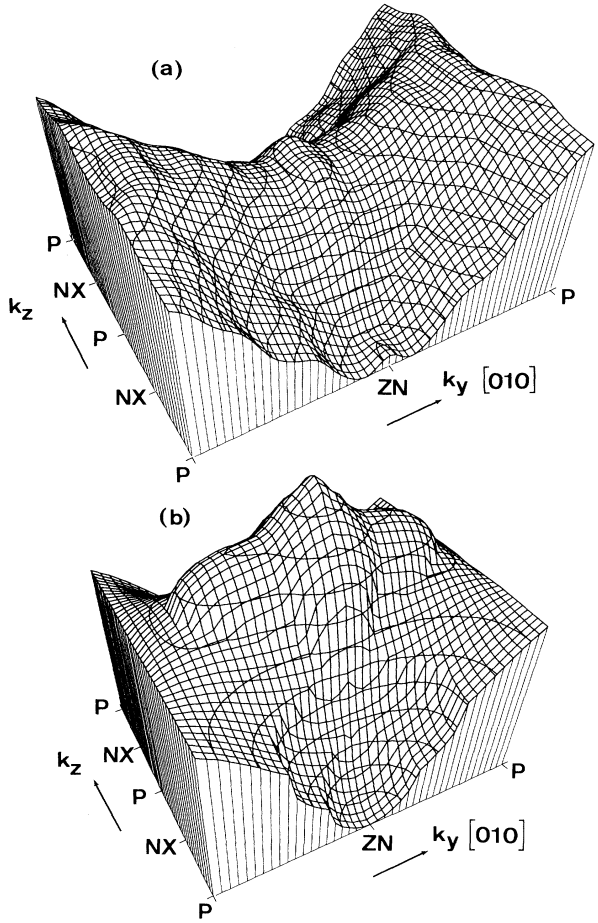

FIG. 4. (a) Measured and (b) calculated LCW distribution for the [101] integration. One unit cell is shown with the projections of the symmetry points in the Brillouin zone. The center of the distribution coincides with the projection of Γ and *N*. The difference between the maximum and the minimum divided by the average value in the LCW distribution amounts to 8.3% for the calculation and 2.5% for the measurement. The k_z axis does not coincide with a crystallographic symmetry direction.

LCW distributions for the [101] integration direction. In the LCW distribution calculated for this integration, the hole surfaces at Z and the electron surfaces at Γ cause a minimum at ZN and a maximum at ΓN, respectively. These features are nicely separated without large positron wave-function effects complicating their interpretation. In the measurement the minimum at ZN is indeed observed. There is thus evidence for the presence of hole surfaces at Z. However, the electron surfaces at Γ are not seen in the experimental distribution; instead, the absolute maximum is located at NX. The application of small shifts to the energy bands near the Fermi level induces a large change of the Fermi-surface topology. The two electron surfaces at Γ are depopulated by an upward shift of 12 mRy, but this is not sufficient to move the maximum in the calculated LCW distribution away from ΓN. The band associated with the large electron pocket possesses little dispersion over a large part of the Brillouin zone. A downward shift by 3 mRy of this band produces an additional electron surface at X. Increasing the shift to 10 mRy yields a large complicated sheet, in addition to a considerable enhancement of the number of states at the Fermi energy. However, the maxima at P and NX observed experimentally are not obtained. The band structure calculated by Norman *et al.*[17] using the linear-muffin-tin-orbitals (LMTO) method yields a similar band at the Fermi energy. From a comparison of both calculations it is inferred that this part of the band structure is particularly sensitive to details of the calculations.

IV. DISCUSSION

Despite the overall similarity between the experimental 2D-ACAR distributions and the projections of the calculated two-photon momentum distribution, a number of discrepancies are observed, which have been described in Sec. III. Several causes can be found, both of an experimental and a theoretical nature; they will be discussed in the following.

From the values of the measured positron lifetimes we have concluded that the spark-cut surface of a sample contains defects which are capable of trapping positrons. Removal of the surface layer by etching successfully reduces the positron trapping, whereas mechanical polishing does not. Mechanical polishing removes the damage caused by spark cutting, but appears to introduce the same amount of defects in the underlying layers. However, in this material we do not see the mere reduction of anisotropic structure observed in other defected materials. We believe that the differences in amplitude of the anisotropic structure at large momenta, as observed in the [001] integration, between theory and experiment on the one hand and between the two samples on the other hand are related to the presence of defects. In URu_2Si_2 various types of defects, which create additional open volume (for instance, vacancies or stacking faults[5]), may act as traps for the positron. In view of the open crystal structure, the wave functions of trapped positrons may not be localized completely. If so, the positron lifetime will be increased only slightly compared to the lifetime in the undistorted lattice. The differences in the measured lifetimes in the samples are indeed small. Therefore, we suggest that the positron charge "leaks" out of the regions near the atomic sites into the defect, reducing the positron density near the atomic nuclei on the one hand, and, on the other hand, maintaining a considerable overlap with the electronic wave functions in the interstitial space. Since the high-momentum contributions mainly originate from the atomiclike oscillations near the atom positions, positron trapping would thus reduce the two-photon momentum distribution at large momenta, whereas this distribution remains unaffected at small momenta. In particular, the anisotropic structure related to the f-electron states, which is visible owing to the high positron density near the U sites, would be reduced by the presence of such defects in the samples. Similar positron behavior was encountered by Hanssen *et al.*[18] in their 2D-ACAR study of the $C1_b$ Heusler alloy NiMnSb. Here, the crystal structure contains empty lattice sites in the unit cell (ordered structural vacancies), which carry an increased positron density. However, the positrons do not become localized completely and still supply information on the Mn d electrons which are responsible for the half-metallic ferromagnetism observed in this compound.

Positrons, which are trapped by vacancy-type defects in a tetragonal crystal lattice, are surrounded by an anisotropic atomic environment. Unless the positron wave function is confined very much to the center of a vacancy, the anisotropy in $\mathbf{r}$ space must cause an anisotropy in the two-photon momentum distribution. As a result, positrons annihilating from defects will yield a featureless but significantly anisotropic 2D-ACAR distribution, in particular if the integration is performed perpendicular to the [001] axis. We think that a partial localization of positrons in defects can thus explain the broad maxima in the anisotropy measured for the [100], [110], and [101] integrations at $p_z = \pm 8$ mrad along the projection of the [001] axis.

Another source of error may be the use of a nonrelativistic expression for the evaluation of the positron-electron overlap integrals in the calculation of the two-photon momentum distribution of Ref. 9.[19] This approximation is not expected to yield significant errors. However, evidence for this is hard to give as a fully relativistic treatment of the positron-annihilation cross section in solids has not been developed until now. More implicitly, the two-photon momentum distribution has been calculated using an independent-particle model, since a reliable many-body theory for such complicated materials is not yet available.[20] Phenomenological models[21] indicate that positron-electron correlation enhances the contribution from s- and p-electron states relative to the more localized d states. Extrapolating this result to the interaction of the positron with the f electrons suggests that positron-electron correlation can explain the observed reduction of anisotropic structure at large momenta. However, it does not account for the sample dependence.

The method adopted to calculate the two-photon momentum distribution involves a spherically symmetric positron wave function inside the muffin-tin spheres for the evaluation of the positron-electron overlap integrals.[19] This procedure is justified since we do not find[9]

significant contributions of nonspherical terms in the calculated positron wave function inside the spheres, whereas the calculation of the wave function does allow such contributions. Nevertheless, the spherical nature of the wave function inside the U muffin-tin sphere is noteworthy in view of the large size of the sphere and the anisotropy of the positron wave function in the interstitial region just outside the sphere, as shown in Fig. 2 of Ref. 9. Nonsphericity of the positron wave function may have been suppressed by the spherical averaging of the electron density and the potential inside the spheres by the warped muffin-tin procedure. In fact, the muffin-tin radius of the U sphere had already been reduced compared to the maximum possible value. Unfortunately, we have not been able to check this point by a band calculation with an even smaller U sphere or with a nonspherical potential inside the sphere.

The LCW distribution calculated by integration of the two-photon momentum distribution along the [101] direction yields a clear projection of the Fermi surface. However, the measured LCW distribution displays a quite different structure, which has a smaller amplitude (see Fig. 4). Positrons annihilating with core electrons as well as positrons trapped by defects usually contribute with a small momentum dependence after LCW folding. Consequently, they merely increase the flat background in the LCW distributions and thus reduce the amplitude of the structure relative to this background. However, the [001] integration measured in the same sample $A1$ closely reproduces the calculated size (4% and 5%, respectively) of the structure caused by the positron wave-function effect. We thus conclude that the reduction of Fermi-surface structure in the [101] integration must be due to either a different Fermi surface topology or many-body interactions or both. Positron-electron correlation usually does not cause such large modifications of the LCW distribution. Electron-electron interactions can be shown[22] to reduce the Fermi-surface discontinuities in the electronic momentum distribution. This effect might be strong enough to explain the small amplitude of the observed Fermi-surface structure.

A direct experimental determination of the occupation number in the first Brillouin zone is possible by performing a reconstruction of the full 3D LCW distribution from its projections.[8] We have shown in Ref. 9 that the positron wave function hardly affects the 3D LCW distribution, so that a reconstruction in principle should be able to give the full Fermi surface with the discontinuities affected by the electronic correlations. Unfortunately, the present experimental data do not allow a reliable reconstruction, as the number of measured integrations is too small and, in addition, the measurements were performed on different samples of varying quality.

We have seen that band shifts of a few mRy improve the agreement with experiment to some extent. These band shifts are considered to compensate for any inaccuracy in the calculation of the band structure, disregarding correlation effects. If successful, the applicability of band theory would be maintained. In the bcc transition metals, for instance, decreasing the energy of the p band by 10–20 mRy relative to the position of the d bands brings the results of band calculations in good agreement with experiments.[23] However, the band structure of URu_2Si_2 yields bands near the Fermi energy with similar character. In that case the relative positions of the bands will be less sensitive to details in the calculation, and the band shifts that can be considered realistic are small. In UPt_3, shifts of the f-like bands as small as 3 mRy were found[7,24] to give a surprisingly good description of the Fermi surface obtained by dHvA experiments. In the case of URu_2Si_2, shifts of a few mRy cannot account for the Fermi-surface projections observed in the 2D-ACAR measurements. Although we cannot completely rule out the possibility that another LDA band calculation would yield good agreement with our experimental data, it appears that a Fermi-surface model supplied by band theory does not apply to URu_2Si_2. Confirmation of this result by dHvA experiments is highly desirable. The possible failure of LDA band theory to give the correct Fermi surface could be explained by strong electron interactions. The crystal-field excitation energy inferred from inelastic neutron-scattering experiments by Broholm *et al.*[25] is 115 K. This is larger than the coherence temperature. Zwicknagl[26] has shown that in this situation the f-electron correlation modifies the Fermi surface resulting from an LDA band calculation. It is remarkable though that the LDA seems to yield a correct Fermi surface in the case of isostructural $CeRu_2Si_2$,[27] for which compound dHvA experiments have been performed;[28] Ce $4f$ electron states generally are more localized than $5f$ states in the analogous U compounds.

We would like to emphasize that the agreement between theory and experiment is rather good with regard to the anisotropy contributed by the f electrons in the 2D-ACAR distributions. The LDA band calculation apparently does well in predicting which f-electron states have the lowest energy and are thus occupied. It would be highly interesting if the electron momentum distribution corresponding to the lowest crystal-field level would be calculated, as an alternative to our band calculation. The positron-annihilation measurement seems to provide a unique opportunity to check the crystal-field model. A range of experiments on URu_2Si_2 have suggested that the magnetic order below 17 K takes the form of a spin-density wave (SDW), as in Cr. The SDW magnetic order originates in the nesting properties of two different Fermi-surface sheets in the paramagnetic state.[29] In the SDW state the energy bands corresponding to these Fermi-surface sheets open up a gap at the Fermi energy. Bonn *et al.*[30] measured the optical conductivity and found clear evidence for the existence of an energy gap: $\Delta E \sim 6$ meV. In a nearly-free-electron model[31] it can be shown that a gap at the Fermi energy smears out the discontinuity in the momentum distribution.[32] The broadening of the Fermi cutoff extends over a width in momentum space given by

$$\Delta p = m^* \frac{\Delta E}{2k_F} , \tag{2}$$

adopting Ry units (k_F is the Fermi wave vector in the free-electron model). Tentatively, we replaced the electron mass by the effective electron mass m^*, which for a

heavy-fermion system results in a relatively large value for Δp. The broadening of the discontinuities should exceed the experimental resolution if one is to expect any measurable effects in the 2D-ACAR distributions upon magnetic ordering by a SDW. However, substitution of realistic values for URu_2Si_2 into Eq. (2) ($k_F \sim 1$ a.u. and $m^* \sim 10$) yields values for Δp that are too small to cause a significant effect.

The slight difference between the 2D-ACAR distributions measured at 6 and 72 K for the [100] integration is attributed to the thermal motion of the positrons. At 72 K, thermal motion yields a contribution to the effective momentum resolution which is approximately equal to the angular resolution in the low-temperature measurement. As a result, the structure observed at 6 K is slightly broadened at 72 K. Broholm *et al.*[25] found that excitations between two crystal-field levels could explain the spin-wave spectrum observed by inelastic neutron scattering in the magnetic state. In addition, the specific heat[12] and thermal expansion[2] show anomalies indicative of crystal-field excitations at 25–30 K. An excited crystal-field level involves f-electron wave functions with a symmetry different from the ground-state level, even though hybridization effects disturb this local f-electron picture in URu_2Si_2. However, the 2D-ACAR experiment shows that the wave functions corresponding to the f states in both levels are similar. Furthermore, the smooth transition from the heavy-fermion Fermi-liquid state to the high-temperature incoherent Kondo state, marked by the maximum in the resistivity at 60 K,[33] does not affect the wave functions of the f-electron states. Moreover, the measurements show that the hybridized f-ligand electron states, provided by the band calculations, are still valid at 72 K. Unfortunately, little information is available about the electronic structure of heavy-fermion systems at high temperature. Angle-resolved photoemission experiments performed by Arko *et al.*[34] suggest that the f-electron states in UPt_3 are still itinerant at 300 K. The localized picture, which is often adopted for the f electrons above the coherency temperature, might not be appropriate for UPt_3 and URu_2Si_2.

V. CONCLUSIONS

We have performed 2D-ACAR experiments on single crystals of URu_2Si_2 for four integration directions at different temperatures. The anisotropy in the 2D-ACAR distributions is reasonably well described by the momentum distribution calculated from a relativistic LDA band structure. Discrepancies are ascribed to the presence of defects in the samples, deduced from the measured positron lifetimes, and to positron-electron correlation. The anisotropic structure observed shows that the band-structure calculation provides the correct shape for the wave functions of the U f-electron states. On the other hand, the structure is found to be rather insensitive to the Fermi-surface topology. An LCW analysis of both theoretical and experimental 2D-ACAR distributions is complicated by slow variations caused by the positron wave function, which dominate over the structure in the LCW distributions due to Fermi-surface projections. Nevertheless, there is evidence that the Fermi surface is incorrectly predicted by theory. The measured integration along the [101] direction displays a minimum where the calculated hole surfaces at Z project, but the electron surfaces centered at Γ, which are predicted by theory, are not observed. The application of small band shifts can not alleviate this discrepancy. The invariance of the 2D-ACAR distribution upon crossing the magnetic phase transition at 17 K does not preclude magnetic order in the form of a spin-density wave. The wave functions of the occupied f states do not appear to be different at 6 and 72 K. Apparently, they are not affected by the coherence transition and crystal-field excitations.

ACKNOWLEDGMENTS

We are indebted to Dr. A. W. Weeber and Dr. L. P. L. M. Rabou for their help in performing the 2D-ACAR experiments, and to Dr. J. de Vries for his positron-lifetime measurements. We would like to thank G. J. Langedijk for technical assistance and B. V. Rajnoch for taking care of the computer facilities. The assistance of G. Hamburg, H. Kooistra, and G. Rietveld with the preparation of the samples is gratefully acknowledged. Discussions with Dr. D. D. Koelling and Professor E. Frikkee were highly appreciated. The work at the Netherlands Energy Research Foundation ECN was part of the research program of the Stichting Fundamenteel Onderzoek der Materie (Foundation for Fundamental Research on Matter) and was made possible by financial support from the Nederlandse Organisatie voor Wetenschappelijk Onderzoek (Netherlands Organization for the Advancement of Research).

[1] M. B. Maple, J. W. Chen, Y. Dalichaouch, T. Kohara, C. Rossel, M. S. Torikachvili, M. W. McElfresh, and J. D. Thompson, Phys. Rev. Lett. **56**, 185 (1986).

[2] A. de Visser, F. E. Kayzel, A. A. Menovsky, J. J. M. Franse, J. van den Berg, and G. J. Nieuwenhuys, Phys. Rev. B **34**, 8168 (1986).

[3] T. T. M. Palstra, A. A. Menovsky, J. van den Berg, A. J. Dirkmaat, P. H. Kes, G. J. Nieuwenhuys, and J. A. Mydosh, Phys. Rev. Lett. **55**, 2727 (1985).

[4] W. Schlabitz, J. Baumann, J. Diesing, W. Krause, G. Neumann, C. D. Bredl, and U. Rauchschwalbe (unpublished).

[5] C. Broholm, J. K. Kjems, W. J. L. Buyers, P. Matthews, T. T. M. Palstra, A. A. Menovsky, and J. A. Mydosh, Phys. Rev. Lett. **58**, 1467 (1987).

[6] D. D. Koelling, Solid State Commun. **43**, 247 (1982).

[7] M. R. Norman, R. C. Albers, A. M. Boring, and N. E. Christensen, Solid State Commun. **68**, 245 (1988).

[8] S. Berko, in *Positron Solid-State Physics,* edited by W. Brandt and A. Dupasquier (North-Holland, Amsterdam, 1983), p. 64.

[9] G. J. Rozing, P. E. Mijnarends, and D. D. Koelling, preced-

ding paper, Phys. Rev. B **43**, 9515 (1991).
[10]A. A. Menovsky, A. C. Moleman, G. E. Snel, T. J. Gortenmulder, H. J. Tan, and T. T. M. Palstra, J. Cryst. Growth **79**, 316 (1986).
[11]P. Zwart, L. P. L. M. Rabou, G. J. Langedijk, A. P. Jeavons, A. P. Kaan, H. J. M. Akkerman, and P. E. Mijnarends, in *Positron Annihilation,* edited by P. C. Jain, R. M. Singru, and K. P. Gopinathan (World Scientific, Singapore, 1985), p. 297; L. P. L. M. Rabou, P. Zwart, G. J. Langedijk, and P. E. Mijnarends, Netherlands Energy Research Foundation ECN, Petten, Report No. ECN-211, 1988 (unpublished).
[12]W. Schlabitz, J. Baumann, B. Politt, U. Rauchschwalbe, H. M. Mayer, U. Ahlheim, and C. D. Bredl, Z. Phys. B **62**, 171 (1986).
[13]F. R. de Boer, J. J. M. Franse, E. Louis, A. A. Menovsky, J. A. Mydosh, T. T. M. Palstra, U. Rauchschwalbe, W. Schlabitz, F. Steglich, and A. de Visser, Physica B **138**, 1 (1986).
[14]D. G. Lock, V. H. C. Crisp, and R. N. West, J. Phys. F **3**, 561 (1973).
[15]An example is the structure observed in early experiments with [001] integration (Ref. 16), which at the time was interpreted as indicative of pipe-shaped Fermi-surface (FS) sheets along [001] centered at the points *X*.
[16]G. J. Rozing, L. P. L. M. Rabou, P. E. Mijnarends, and A. A. Menovsky, in *Positron Annihilation,* edited by L. Dorikens-Vanpraet, M. Dorikens, and D. Segers (World Scientific, Singapore, 1989), p. 233.
[17]M. R. Norman, T. Oguchi, and A. J. Freeman, Phys. Rev. B **38**, 11 193 (1988).
[18]K. E. H. M. Hanssen and P. E. Mijnarends, Phys. Rev. B **34**, 5009 (1986); K. E. H. M. Hanssen, L. P. L. M. Rabou, P. E. Mijnarends, and K. H. J. Buschow, *ibid.* **42**, 1533 (1990).
[19]G. J. Rozing, P. E. Mijnarends, and R. Benedek, Phys. Rev. B **43**, 6996 (1991).
[20]J. Arponen and E. Pajanne, in *Positron Annihilation,* edited by P. C. Jain, R. M. Singru, and K. P. Gopinathan (World Scientific, Singapore, 1985), p. 21.
[21]See, for instance, A. M. Manuel, A. K. Singh, T. Jarlborg, P. Genoud, L. Hoffmann, and M. Peter, in *Positron Annihilation,* edited by L. Dorikens-Vapreaet, M. Dorikens, and D. Segers (World Scientific, Singapore, 1989), p. 109.
[22]J. P. Carbotte, in Ref. 8, p. 32.
[23]See, for instance, D. M. Bylander and L. Kleinman, Phys. Rev. B **29**, 1534 (1984).
[24]N. E. Christensen, O. K. Andersen, O. Gunnarson, and O. Jepsen, J. Magn. Magn. Mater. **76&77**, 23 (1988).
[25]C. Broholm, H. Lin, P. T. Matthews, T. E. Mason, W. J. L. Buyers, M. F. Collins, A. A. Menovsky, J. A. Mydosh, and J. K. Kjems (unpublished).
[26]G. Zwicknagl, J. Magn. Magn. Mater. **76&77**, 16 (1988).
[27]G. Zwicknagl, E. Runge, and N. E. Christensen, Physica B **163**, 97 (1990).
[28]G. G. Lonzarich, J. Magn. Magn. Mater. **76&77**, 1 (1988).
[29]The magnetism of Cr was recently reviewed by E. Fawcett, Rev. Mod. Phys. **60**, 209 (1988).
[30]D. A. Bonn, J. D. Garrett, and T. Timusk, Phys. Rev. Lett. **61**, 1305 (1988).
[31]S. Berko and J. S. Plaskett, Phys. Rev. **112**, 1877 (1958).
[32]J. Friedel and M. Peter, Europhys. Lett. **8**, 79 (1989).
[33]T. T. M. Palstra, A. A. Menovsky, and J. A. Mydosh, Phys. Rev. B **33**, 6527 (1986).
[34]A. J. Arko, P. Armstrong, and M. Wire, Physica B **163**, 167 (1990).